Solution-processable dendric triphenylamine nonamers as hole-transporting and hole-injection materials for organic light-emitting devices

Musubu Ichikawa*, Keiko Hibino, Norimasa Yokoyama[†], Tetsuzo Miki[†], Toshiki Koyama and Yoshio Taniguchi

Department of Functional Polymer Science, Faculty of Textile Science and technology, Shinshu University, 3-15-1 Tokita, Ueda City, Nagano 386-8567, Japan

[†]*Hodogaya Chemical Co., Ltd, 45 Miyukigaoka, Tsukuba City, Ibaraki 305-0841, Japan*

(Received)

We demonstrated two solution-processable triphenylamine dendric nonamers: the N-atom-centered nonamer (TPA9-1) and the phenyl-centered nonamer (TPA9-2). The materials were found to have high glass transition temperature (Tg) up to almost 200°C. The fractional difference of the central units of the molecular structures caused different adaptability due to the different ionization potentials (Ip). TPA9-1 (N-atom-centered), whose Ip was smaller than that of TPA9-2 (phenyl-centered), was suitable as hole injection layer material, and TPA9-2 was suitable as hole-transporting layer material. Computational chemistry provides a ready explanation for the Ip difference between the two materials.

Keywords: triphenylamine; dendrimer; hole transport; organic light-emitting diode; solution processable

*Corresponding author at: *Department of Functional Polymer Science, Faculty of Textile Science and technology, Shinshu University, 3-15-1 Tokita, Ueda City, Nagano 386-8567, Japan*

Tel: +81-268-21-5498; Fax: +81-268-21-5413

Email address: musubu@shinshu-u.ac.jp

1. **Introduction**

Organic light-emitting devices (OLEDs) have received a lot of attention because of their potential applications in flat-panel displays and lighting. In general, OLEDs are composed of functionally divided multilayers such as hole injection, hole-transporting (HT), emissive, hole-blocking, electron-transporting layers, and so on. This structure enables the optimal charge balance essential to high electroluminescence (EL) efficiency.[1, 2] In the last decade, many kinds of amorphous molecular semiconductor materials,[3, 4] working as HT materials[5-9] and ET materials,[10-16] have been proposed.

It has been established that the triphenylamine group is one of the most valuable groups for HT functions in organic semiconductors. In fact, some triphenylamines derivatives such as N,N'-diphenyl N,N'-bis(*m*-toly) benzidine (TPD) and N,N'-dinaphthyl N,N'-diphenyl benzidine (NPB)[5] are already in common use as HT materials for OLEDs. The electron-donating nature of triarylamines (including triphenylamine) is the basis of its good hole-transporting properties. Though higher molecular weight with rigid building blocks like arylene leads to higher glass transition temperature (Tg), which is important for long-term durability of OLEDs, it also causes poorer solubility. Dendric or starburst molecules have both high Tg and high solubility. In fact, the starburst triphenylamines developed by Shirota *et al*. are conventional OLED materials with high Tg.[7, 17, 18] In this study, we describe two new dendric triphenylamine nonamers with solution processability and high Tg. We also describe an effective modulation of the highest occupied molecular orbital (HOMO) that controls HT and

hole injection properties by altering a small fraction of the molecular structure.

2. Experimental

2.1 Measurements and Calculation

^{1}H-NMR spectra were recorded either on a JEOL JNM-EX270 spectrometer (270 MHz) or a Bruker AVANCE spectrometer (400 MHz). Elemental analysis was carried out with a Yanaco MT-3 CHNcoder. Thermal analysis was done on a Seiko Instruments DSC-6200 at a heating rate of 10°C/min for differential scanning calorimetry in nitrogen. UV and visible absorption spectra and fluorescence spectra were recorded with a Shimadzu UV-3150 spectrophotometer and a JASCO FP-750 spectrofluorometer, respectively. Ip was measured with a Riken Keiki AC-2 photoelectron emission spectrometer, and the Ea was estimated from the Ip and the band gap, which were determined by the absorption edge of the UV and the visible absorption spectrum of the neat thin film. Neat thin films prepared by spin coating on quartz glasses from each solution at atmosphere were used as samples for UV-visible absorption, fluorescence, and photoelectron emission spectroscopy. Mass spectroscopic analysis was carried out with a matrix-assisted laser desorption ionization time-of-flight (MALDI-TOF) mass spectrometer (Applied Biosystems, Voyager-DE PRO). Surface morphologies of thin-films were evaluated with an AFM (SII Nanotechnology, SPA-400). Computational calculations were carried out on a commercial quantum chemistry package (Gaussian 03) with a Hatree-Fock method of a 6-31G(d) basis set for obtaining the molecular optimal geometries. Using the optimal geometries, a density functional theory (B3LYP) of a 6-311G+(2d,p) basis set visualized molecular orbitals (MOs) and estimated

energies of MOs.

2.2 Materials

Figure 1 shows the molecular structures of triphenylamine dendric nonamers TPA9-1 and TPA9-2. The nonamers (TPA9s) were synthesized according to the procedures shown in Scheme 1. The details of the syntheses are described below. TPA9-1 and TPA9-2 were synthesized and purified and were used without any further purification. Their identities were confirmed by elemental analysis, ^{1}H-NMR, and MALDI-TOF mass spectroscopy. Other OLED chemicals used in this study were from Nippon Steel Chemical (CuPc; Copper phthalocyanine, NPB, Alq) and H. W. Sands (mMTDATA; 4,4',4''-tris(3-methylphenylphenylamino)triphenylamine). These materials were used with no further purification because they were sublimation grade.

2.3 Synthesis

2.3.1 Synthesis of 4'-iodo-N,N-diphenylbiphenyl-4-amine (IB-DPA)

Diphenylamine (50.0 g, 0.295 mol), 4,4'-diiodobiphenyl (167.8 g, 0.413 mol), Cu (4.70 g, 0.074 mol), dried K_2CO_3 (57.1 g, 0.413 mol), and $NaHSO_3$ (4.6 g, 0.044 mol) in 14.6 ml *n*-dodecane and 44.6 ml *p*-xylene were stirred in N_2 gas. Then, the temperature was increased to 150°C to remove the *p*-xylene. After that, the temperature was increased again to 220°C. The mixture was stirred continuously for 9.5 hours, and then 440 ml tolene was slowly added to the mixture as it was cooled. After 1-hour-refluxing of the mixture, it was filtered at 80°C. Then, 150 ml cyclohexane and 150 ml *n*-hexane were added to the filtrate precipitated IB-DPA. The precipitate was isolated by filtration and vacuum dried. Silica gel column chromatography (tolene/*n*-hexane = 1/6) produced 69.4

g of pure IB-DPA powder with a 50.6% yield. δ_H (270 MHz, $CDCl_3$) 6.986 (2H, t, J 7.2 Hz), 7.037-7.086(6H, m), 7.184-7.264 (6H, m), 7.370 (2H, d, J 9.2 Hz), 7.668 (2H, d, J 8.6 Hz).

2.3.2 Synthesis of N,N-bis(4'-diphenylamino-biphenyl-4-yl)amine (B(DPAB)A)

Benzamide (4.08 g, 33.7 mmol), IB-DPA (15.84 g, 35.4 mmol), Cu (0.54 g, 8.5 mmol), dry K_2CO_3 (6.99 g, 50.6 mmol), and $NaHSO_3$ (0.53 g, 5.06 mmol) in 1 ml *n*-dodecane and 5 ml *p*-xylene were stirred under N_2 gas at 180°C for 3 hours. The same amounts of IB-DPA, Cu, and dried K_2CO_3 were added to the mixture, and then the mixture was stirred at 195°C for 8 hours. After decreasing the temperature to 110°C, 270 ml of tolene was dropped into the mixture, which was then refluxed for 1 hour. Debenzylation with 3.78 g (67.4 mmol) and 40 ml 2-propanol was carried out at 70°C. After removing 2-propanol at 90°C, the mixture was refluxed for 1 hour with an additional of 40 ml tolene. After filtration at 50°C the filtrate was dried to obtaine crude B(DPAB)A powder. The crude powder was washed with acetone, and dissolved in 50 ml tetrahydrofuran to precipitate in *n*-hexane/acetone (200 ml/20 ml). The precipitation produced 16.62 g of pure B(DPAB)A powder with a 72.7% yield. δ_H (400 MHz, DMSO-d_6) 7.017-7.059 (16H, m), 7.170 (4H, d, J 8.6 Hz), 7.305 (8H, t, J 8 Hz), 7.536 (4H, d, J 8.4 Hz), 7.547 (4H, d, J 8.4 Hz), 8.405 (1H, s).

2.3.3 Synthesis of 4,4',4"-tris[N,N-bis(4'-diphenylaminobiphenyl-4-yl)amino] triphenylamine (TPA9-1)

Tris(4-bromophenyl)amine (0.23 g, 0.48 mmol), B(DPAB)A (1.00 g, 1.52 mmol), *tert*-butolate sodium (0.13 g, 1.34 mmol), palladium (II) acetate (0.01 g, 0.04 mmol),

$NaHSO_3$ (0.003 g, 0.033 mmol), and tris(tert-butyl)phosphine (16 μl, 0.038 mmol) in 10 ml dry tolene were stirred in N_2 gas at 110°C for 3 hours. After refluxing for 1 hour with an additional 60 ml of tolene, the mixture was filtered at 80°C. Another precipitate appeared in the filtration when the temperature of the filtration went down. The precipitate was isolated with a filter. Silica gel chromatography ($CHCl_3$/*n*-hexane = 5/3) produced 0.66 g of pure TPA9-1 powder with a 62.3% yield. Elemental analysis: calc. for $C_{162}H_{120}N_{10}$: C=88.17, H=5.94, N=6.35. Found: C=87.85, H=5.98, N=6.17. *m/z* (MALDI-TOF) 2205.86 (M+ requires 2205.97). δ_H (400 MHz, benzene-d_6) 6.853 (12H, t, J 7.8 Hz), 7.053 (24H, d, J 6.8 Hz), 7.111 (42H, d, J 8.6 Hz), 7.185 (6H, d, J 8.8 Hz), 7.233 (12H, d, J 8.6 Hz), 7.373 (12H, d, J 8.4 Hz), 7.410 (12H, d, J 8.8 Hz).

2.3.4 Synthesis of 4,4',4''-Tris[N,N-bis(4'-diphenylaminobiphenyl-4-yl)amino] triphenybenzene (TPA9-2)

1,3,5-Tris(4-bromophenyl)benzene (1.68 g, 3.09 mmol), B(DPAB)A (8.33 g, 10.2 mmol), *tert*-butolate sodium (1.77 g, 18.4 mmol), palladium (II) acetate (0.010 g, 0.046 mmol), and tris(tert-butyl)phosphine (0.036 g, 0.18 mmol) in 50 ml dry tolene were stirred and refluxed under N_2 gas for 9 hours. The mixture was filtered at 80°C. Another precipitate appeared in the filtration when the filtration cooled. The precipitate was isolated with a filter, and washed twice with 100 ml of water and 100 ml of methanol, and then 2-time recrystallization from tolene and washing with refluxed methanol produced 3.79 g of pure TPA9-2 powder with a 54.1% yield. Elemental analysis: calc. for $C_{168}H_{123}N_9$: C=88.97, H=5.47, N=5.56. Found: C=88.64, H=5.67, N=5.50. *m/z* (MALDI-TOF) 2267.12 (MH+ requires 2267.00). δ_H (400 MHz, $CDCl_3$) 7.019 (12H, t, J 7.3 Hz), 7.124 (36H, d, J 8.3 Hz), 7.207-7.278 (42H, m), 7.463 (12H, d, J 8.6 Hz),

7.492 (12H, d, J 8.6 Hz), 7.613 (6H, d, J 8.6 Hz), 7.736 (3H, s).

2.4 Fabrication and Measurement of OLEDs

OLEDs fabricated in this experiment have an indium-tin-oxide (ITO)/organic multilayer structure (total thickness: 100 nm)/cathode (200 nm). An ITO-coated glass substrate with a sheet resistance of 14 Ω/square treated in advance with O_2-plasma for 5 minutes was used as the substrate and anode. All layers except the TPA9s were sequentially deposited on the substrate at a pressure of 6×10^{-4} Pa or less. 50-nm-thick TPA9 layers were prepared with a spin coater at a spin rate of 4100 rpm for 30 sec from a 2wt% 1,1,2-trichloroethane solution for TPA9-1 and at a spin rate of 2430 rpm for 30 sec from a 2wt% cyclohexanone solution for TPA9-2. The 20-nm-thick TPA9-1 layers used as hole injection layers were prepared from a 1wt% 1,1,2-trichloroethane solution in the same spinning conditions. The emissive area of the device was 2×2 mm^2. The current density-applied voltage-luminance characteristics of OLEDs were measured with a commercial OLED characteristics measurement system (Precise Gauge, EL1003).

3. Results and Discussion

Figure 1 shows the molecular structures of triphenylamine dendric nonamers TPA9-1 and TPA9-2. The difference between the molecules is in the center unit, which is either a nitrogen atom or a phenyl group. Table 1 shows thermal, spectroscopic, and electronic properties of TPA9s in solid or thin-film states. As shown in the table, the two materials exhibited similar properties. Since the ionization potentials (Ip) of the materials, at around 5.1 – 5.3 eV, are compatible with the work function of ITO used as an anode, it

was expected that TPA9s would exhibit good hole accepting from the anode. In addition, the small electron affinities (Ea), which were estimated by the Ip and optical band gap, suggest that there are electron confinements in the emissive layers.

TPA9s are very stable in their glass states; Tgs of the materials were 188°C for TPA9-1 and 194°C for TPA9-2. The melting points (Tm) of the materials were close to their Tgs. Because the molecular weights of TPA9-1 (2206.75) and -2 (2267.83) are similar to each other and both of their center units are 3-way bonding, the similar Tgs and Tms of TPA9s probably indicate that the actual steric molecular structures in the amorphous solid state resemble each other. As illustrated in Fig. 2, the computational molecular geometries of TPA9s, clearly show that the TPA9s' structures are indeed very similar.

Figure 3 shows atomic force microscopy (AFM) images of the surface morphologies of the solution-processed TPA9-2 thin-film on an ITO substrate together with a bare ITO. It can be seen, by comparing Figs. 3(a) and (b), that no significant morphological changes appeared after thermal treatment at 180°C for 60 min; the average surface roughness (Ra) and peak-to-valley roughness (Rp-v) of the post-treatment thin-films were 0.39 and 3.9 nm, respectively. In addition, in comparison with Fig. 3(d), the AFM image of the bare ITO surface, Figs. 3(a) and (b) clearly indicate that the surface became smoother. Ra and Rp-v of the bare ITO were 1.7 and 13.5 nm, respectively. By contrast, the Ra and Rp-v for the solution-processed TPA9-1 thin-film were 0.35 and 4.2 nm, respectively, meaning that the surface of TPA9-1 was also smooth as shown in Fig. 3(c).

Figure 4(a) shows current density-voltage (*J-V*) characteristics of OLEDs that use a 50-nm-thick TPA9 layer as an HT layer (HTL) and of a control device, whose HTL was NPB. All the devices in our experiment used 50-nm-thick tris(8-quinolinato)aluminum (Alq) as an electron-transporting and emissive layer, and LiF (0.5 nm)/Al (200 nm) as an electron-injection buffer and a cathode. The device structure and the chemical structures used in the materials are represented in Fig. 1. The TPA9-2 device showed slightly better *J-V* characteristics than the control device (NPB/Alq). The TPA9-1 device, on the other hand, exhibited poor *J-V* performance compared with the control device. As shown in Fig. 4(b), luminance-current density (*L-J*) characteristic of the TPA9-2 device was comparable to that of the control device, whereas that of the TPA9-1 device was not as good as the control. Therefore, TPA9-2 is as good as NPB from the viewpoint of device performance and has the added advantage of a higher Tg (194°C). Furthermore, as shown in Figure 5, the EL spectrum from the device with TPA9-2 was completely same to that from the reference device. Namely, recombination of hole and electron occurs in the Alq layer in case of the TPA9-2 device as same as in case of the reference device.

On the other hand, TPA9-1 showed poor *J-V-L* performance. TPA9-1's higher electron donation property is probably the reason for TPA9-1's poor performance as an HT material because TPA9-1 has smaller Ip than TPA9-2. The central nitrogen atom and the other nitrogen atom connected through the phenyl ring looks like *p*-phenylenediamine, which is well known as a high electron donating molecule. For example, N,N,N',N'-tetramethyl-*p*-phenylenediamine, a derivative of *p*-phenylenediamine, in a methanol glass at 77 K is photo-ionized with a radiation of 4.75-eV light.[19] Another

relevant feature is the surface of the highest occupied molecular orbitals (HOMOs) of TPA9s, which are also shown in Figure 2. As can be seen, the HOMO of TPA9-1 is localized at the molecule's central unit, which is composed of the center nitrogen atom and three triphenylamine groups connected to the N atom with a C_3 symmetry. The energy level of the HOMO was 0.33 eV higher than those of double-degenerated occupied MOs adjacent to the HOMO, where both double-degenerated occupied MOs were found in peripheral units with a C_1 symmetry. In contrast, the HOMO of TPA9-2 is almost triple-degenerated, and each triple-generated HOMO is located not at the center unit but in peripheral units, where two MOs with a C_1 symmetry are degenerated and the remaining MOs, each with a C_3 symmetry, are slightly deeper (0.003 eV) than the HOMO of TPA9-2. In other words, the central unit, which is like tris(4-(N,N-diphenylamino)phenyl)amine, enhances the electron-donation property of TPA9-1.

Figure 6(a) shows the *J-V* characteristics of OLEDs with hole injection layers (HILs) made of TPA9-1 and other materials. The device structure is ITO/HIL (20 nm)/TPD (30 nm)/Alq (50 nm)/Mg-Ag alloy (200 nm), where the Mg-Ag alloy is formed by thermal deposition at 9:1 volume ratio. As shown in the figure, the TPA9-1 HIL device showed comparable *J-V* characteristics to the mMTDATA-HIL reference device but less favorable than that of the CuPc-HIL reference device. Figure 6(b) shows the current efficiency-current density (η-*J*) characteristics of the devices. The TPA9-1-HIL device showed better η-*J* performance than the CuPc-HIL reference device. The colorless high optical transparency of the TPA9-1 thin-film probably causes the advanced η-*J* characteristic.

4. Conclusions

We described two new triphenylamine dendric nonamers that were solution-processable and had Tgs of almost 200°C. The thin-films of the nonamers showed excellent thermal stability. In other words, no morphological change occurred even after the 180°C treatment. The phenyl-centered nonamer (TPA9-2) can be used as an HTL material. The other compound, the N-atom-centered nonamer (TPA9-1), showed poor performance as an HTL material compared with TPA9-2 but exhibited HIL material properties comparable to other good HIL materials such as CuPc and mMTDATA. The difference in the properties results from the fractional difference of the central units of the molecular structures. The fractional structure difference causes the differences in ionization potential. Computational chemistry supports the idea that the *p*-phenylenediamine-like structure affected ionization potential.

Acknowledgements

This work was supported by the Cooperative Link for Unique Science and Technology for Economic Revitalization (*CLUSTER*) of Japan's Ministry of Education, Culture, Sports, Science and Technology. It was also supported by the Ministry's 21st Century COE program.

References

[1] C. W. Tang, S. A. VanSlyke, Appl. Phys. Lett. 51 (1987) 913.

[2] C. Adachi, T. Tsutsui, S. Saito, Appl. Phys. Lett. 57 (1990) 531.

[3] Y. Shirota, J. Mater. Chem. 10 (2000) 1.

[4] U. Mitschke, P. Baeuerle, J. Mater. Chem. 10 (2000) 1471

[5] S. A. VanSlyke, C. H. Chen, C. W. Tang, Appl. Phys. Lett. 69 (1996) 2160.

[6] M. Thelakkat, H.-W. Schmidt, Adv. Mater. 10 (1998) 219.

[7] K. Katsuma, Y. Shirota, Adv. Mater. 10 (1998) 223.

[8] H. Tanaka, S. Tokito, Y. Taga, A. Okada, Chem. Commun. (1996) 2175.

[9] U. Bach, K. D. Cloedt, H. Spreitzer, M. Grätzel, Adv. Mater. 12 (2000) 1060.

[10] C. Adachi, T. Tsutsui, S. Saito, Appl. Phys. Lett. 55 (1989) 1489.

[11] Y. Hamada, C. Adachi, T. Tsutsui, S. Saito, Jpn. J. Appl. Phys. 31 (1992) 1812.

[12] K. Tamao, M. Uchida, T. Izumizawa, K. Furukawa, S. Yamaguchi, J. Am. Chem. Soc. 118 (1996) 11974.

[13] M. Uchida, T. Izumizawa, T. Nakano, S. Yamaguchi, K. Tamao, K. Furukawa, Chem. Mater. 13 (2001) 2680.

[14] J. Bettenhausen, P. Strohriegl, Adv. Mater. 8 (1996) 507.

[15] S. B. Heidenhain, Y. Sakamoto, T. Suzuki, A. Miura, H. Fujikawa, T. Mor, S. Tokito, Y. Taga, J. Am. Chem. Soc. 122 (2000) 10240.

[16] M. Ichikawa, T. Kawaguchi, K. Kobayashi, T. Miki, K. Furukawa, T. Koyama, Y. Taniguchi, J. Mater. Chem. 16 (2006) 221.

[17] H. Inada, Y. Shirota, J. Mater. Chem. 3 (1993) 319.

[18] Y. Kuwabara, H. Ogawa, H. Inada, N. Noma, Y. Shirota, Adv. Mater. 6 (1994) 677.

[19] A. Bernas, G. M., D. Grand, P. G., Chem. Phys. Lett. 17 (1972) 439.

Captions

Table 1. Thermal, spectroscopic, and electronic properties of TPA9s.

Scheme 1. Synthetic route of the TPA9s.

Figure 1. Chemical structures of materials used and structure of the device in this study

Figure 2. Molecular structures and HOMOs of TPA9s as obtained by quantum mechanical chemistry.

Figure 3. AFM images of TPA9-2 thin-films on ITO: (a) as-prepared, (b) after annealing at 180°C for 1 hour. (c) as-prepared TPA9-1 thin film on ITO and (d) pristine ITO surface.

Figure 4. (a) Current density-voltage and (b) luminance-current density characteristics of OLEDs with TPA9s or NPB as an HTL. The same symbols are used in panel (b).

Figure 5. EL spectra from the OLED with TPA9-2 (solid line) and NPB (dashed line) as an HTL at the current density of 160 mA/cm^2.

Figure 6. (a) Current density-voltage and (b) current efficiency-current density characteristics of OLEDs with TPA9-1 or other materials as an HIL. The same symbols are used in panel (b). Device structure is ITO/HIL(20 nm)/TPD(30 nm)/Alq(50 nm)/MgAg.

Table 1. Thermal, spectroscopic, and electronic properties of TPA9s.

Material	Tg (°C)	Tm (°C)	λ_{max}^{abs} (nm)	λ_{max}^{PL} (nm)	Ip (eV)	Ea (eV)
TPA9-1	188	200	363	450	5.12	2.12
TPA9-2	194	215	365	421	5.32	2.26

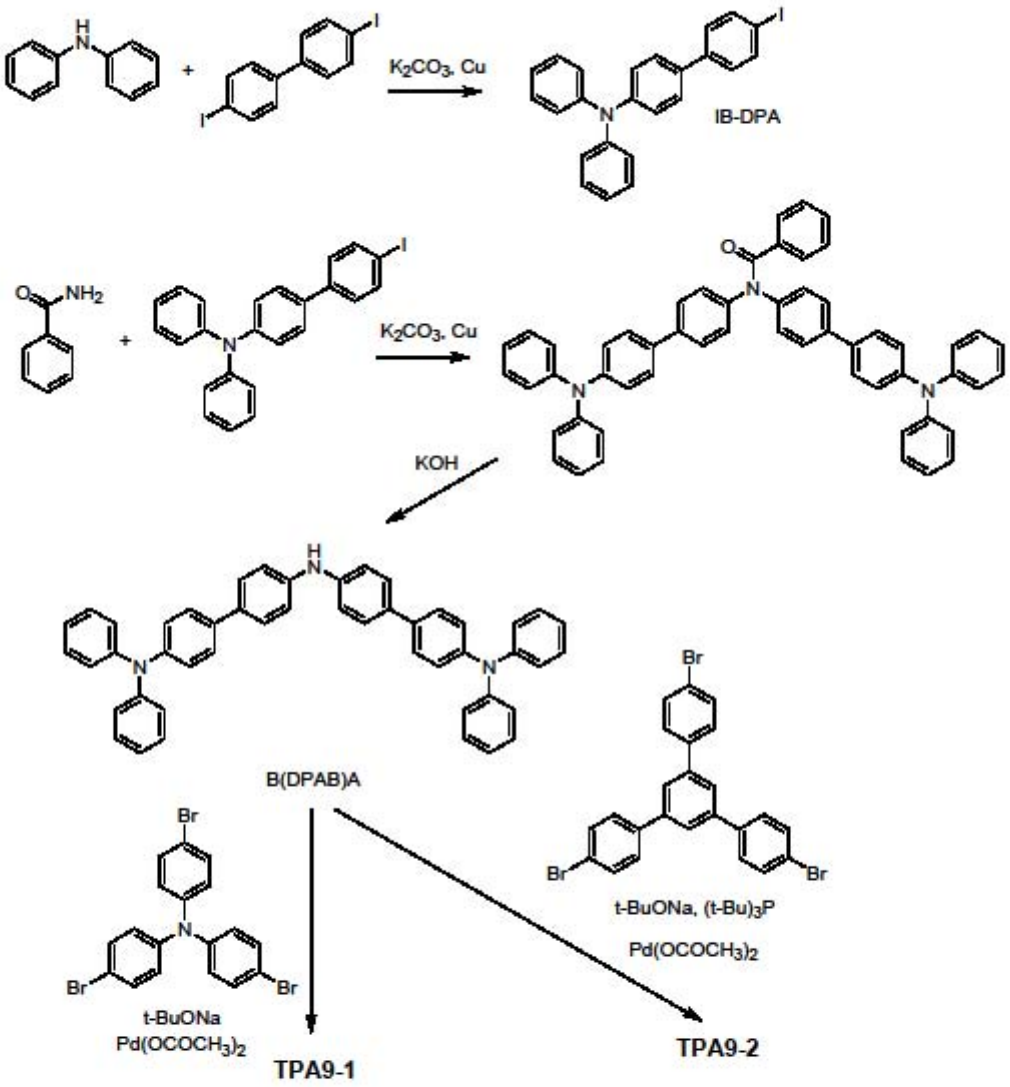
K2CO3, Cu
IB-DPA
K2CO3, Cu
KOH
B(DPAB)A
t-BuONa
Pd(OCOCH3)2
TPA9-1
t-BuONa, (t-Bu)3P
Pd(OCOCH3)2
TPA9-2

Scheme 1

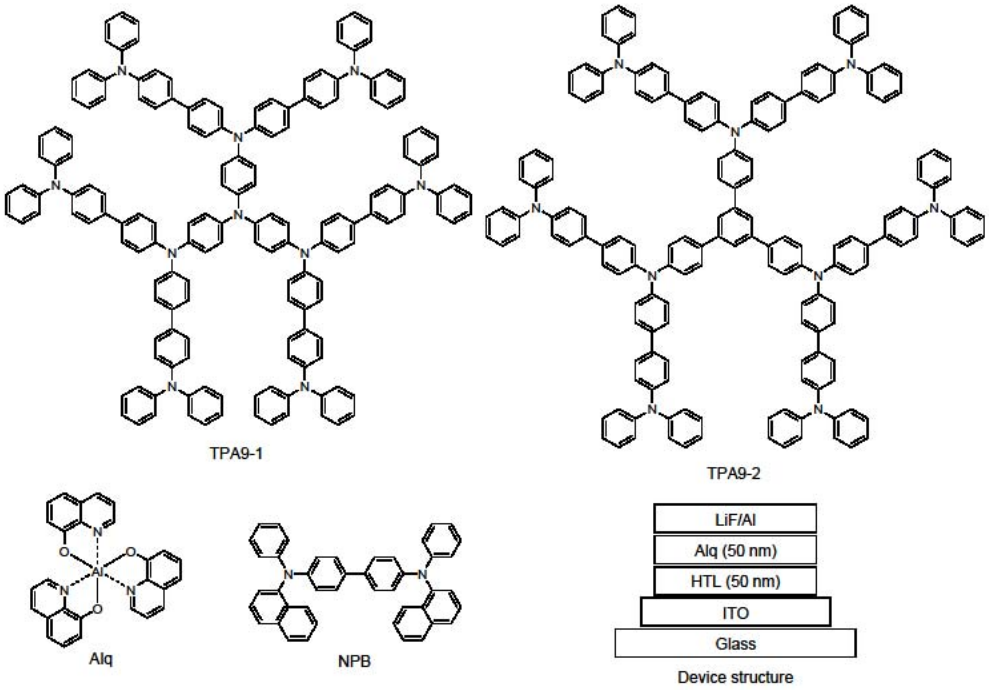
TPA9-1
TPA9-2
Alq
NPB
LiF/Al
Alq (50 nm)
HTL (50 nm)
ITO
Glass
Device structure

Fig. 1

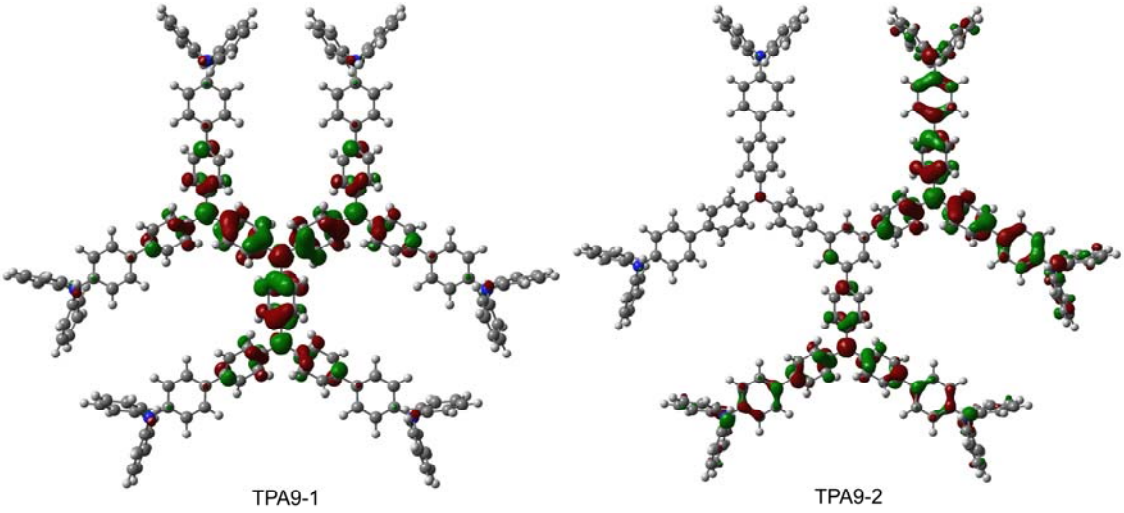

Fig. 2

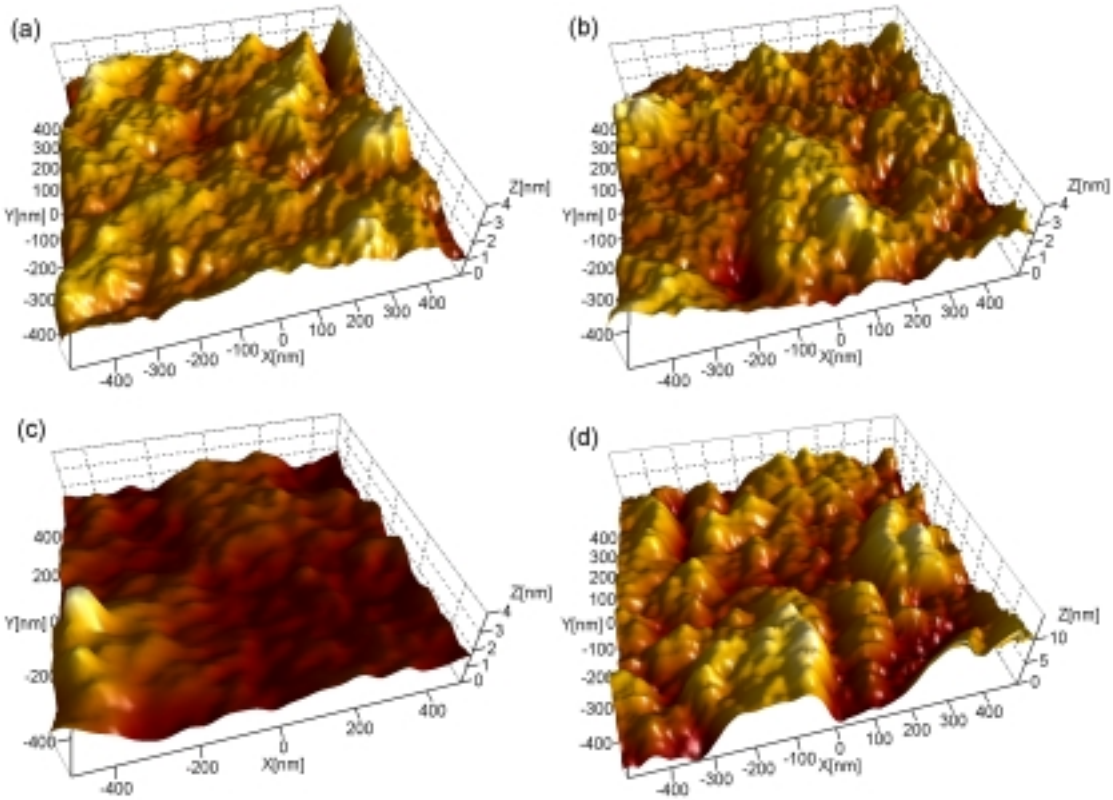

Fig. 3

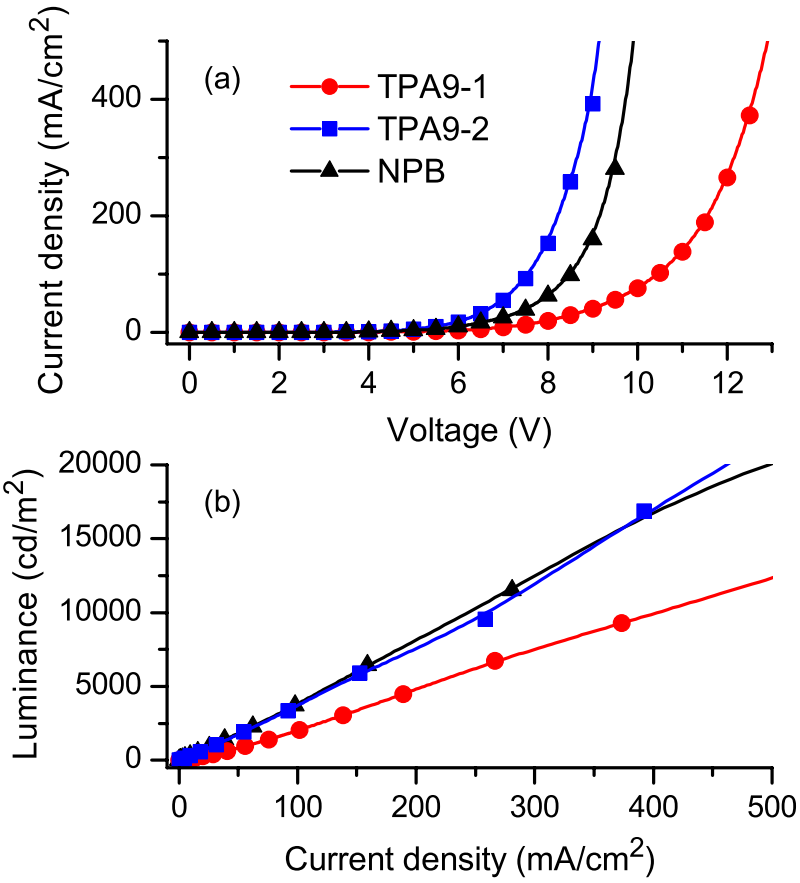
(a)
TPA9-1
TPA9-2
NPB
Current density (mA/cm2)
Voltage (V)
(b)
Luminance (cd/m2)
Current density (mA/cm2)

Fig. 4

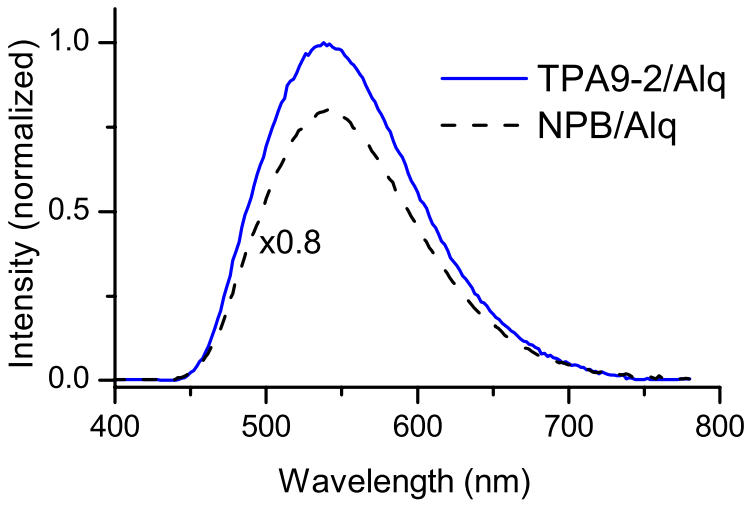
Intensity (normalized)
1.0
0.5
0.0
400
500
600
700
800
Wavelength (nm)
TPA9-2/Alq
NPB/Alq
x0.8

Fig. 5

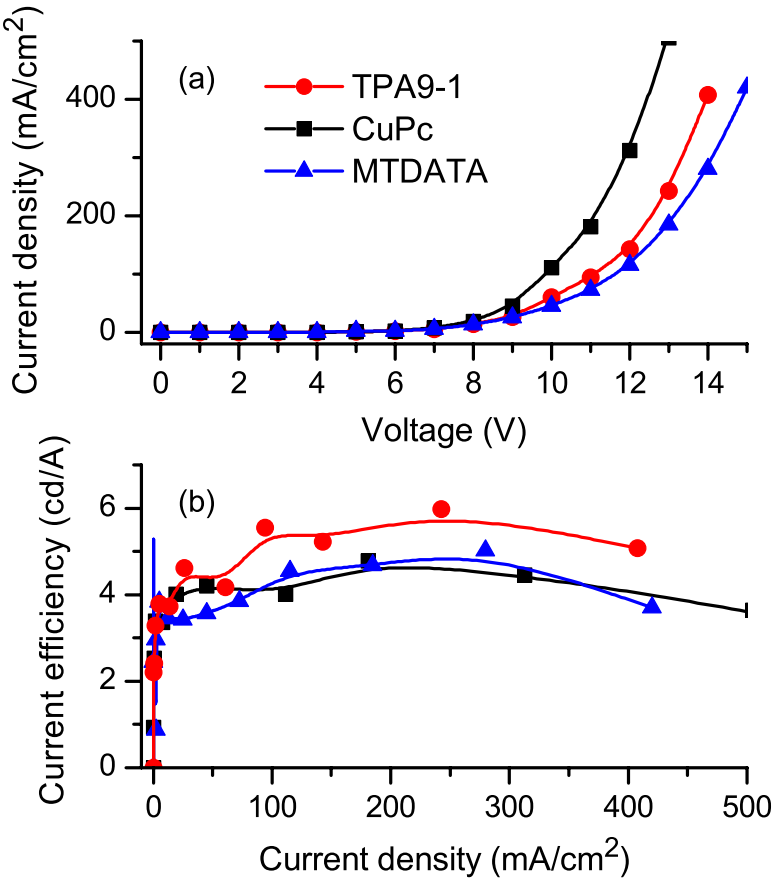
(a)
TPA9-1
CuPc
MTDATA
Current density (mA/cm2)
Voltage (V)
(b)
Current efficiency (cd/A)
Current density (mA/cm2)

Fig. 6